Kokka, Alexander; Pulli, Tomi; Ferrero, Alejandro; Dekker, Paul; Thorseth, Anders; Kliment, Petr; Klej, Adam; Gerloff, Thorsten; Ludwig, Klaus; Poikonen, Tuomas; Ikonen, Erkki

Validation of the fisheye camera method for spatial non-uniformity corrections in luminous flux measurements with integrating spheres

Published in:
Metrologia

DOI:
10.1088/1681-7575/ab17fe

Published: 18/06/2019

Document Version
Publisher's PDF, also known as Version of record

Metrologia

PAPER • **OPEN ACCESS**

Validation of the fisheye camera method for spatial non-uniformity corrections in luminous flux measurements with integrating spheres

To cite this article: Alexander Kokka *et al* 2019 *Metrologia* **56** 045002

OPEN ACCESS
IOP Publishing
Metrologia

Metrologia **56** (2019) 045002 (9pp)
https://doi.org/10.1088/1681-7575/ab17fe

Validation of the fisheye camera method for spatial non-uniformity corrections in luminous flux measurements with integrating spheres

Alexander Kokka[1,2], Tomi Pulli[1], Alejandro Ferrero[3], Paul Dekker[4], Anders Thorseth[5], Petr Kliment[6], Adam Klej[7], Thorsten Gerloff[2], Klaus Ludwig[8], Tuomas Poikonen[9] and Erkki Ikonen[1,9]

[1] Metrology Research Institute, Aalto University, Espoo, Finland
[2] Physikalisch-Technische Bundesanstalt, Braunschweig, Germany
[3] CSIC, Instituto de Óptica 'Daza de Valdés', Madrid, Spain
[4] VSL, Delft, The Netherlands
[5] DTU Fotonik, Technical University of Denmark, Roskilde, Denmark
[6] Czech Metrology Institute, Prague, Czech Republic
[7] Philips Lighting, Eindhoven, The Netherlands
[8] OSRAM, Augsburg, Germany
[9] VTT Technical Research Centre of Finland Ltd, Espoo, Finland

E-mail: alexander.kokka@aalto.fi

Received 5 November 2018, revised 21 March 2019
Accepted for publication 10 April 2019
Published 18 June 2019

Abstract

In this paper, the fisheye camera method is validated for spatial non-uniformity corrections in luminous flux measurements with integrating spheres. The method was tested in eight integrating spheres with six LED lamps, and the determined angular intensity distributions and spatial non-uniformity correction factors were compared with the results of five goniophotometers. The average closeness score, describing the similarity between any two distributions, was 94.6 out of 100 for the distributions obtained using the fisheye camera method when compared with the goniophotometric results. The average closeness score for the five goniophotometers, when each goniophotometer was compared with the other four, was 96.6. On average, the relative deviation between the two methods was 0.05% when calculating the spatial corrections. The most significant sources of uncertainty for the fisheye camera method were large, view-obstructing sphere elements residing close to the camera port.

Keywords: fisheye camera method, integrating sphere, luminous flux, spatial correction, angular intensity distribution, photometry, measurement uncertainty

(Some figures may appear in colour only in the online journal)

1. Introduction

The angular intensity distribution describes the far-field radiation pattern of a light source. It is one of the key metrics of a lighting product, and such distributions are frequently measured during the development stage of new lamps and luminaires. Among their other applications, relative angular intensity distributions are used in luminous flux measurements [1] with integrating spheres to reduce measurement uncertainty due to the spatial non-uniformity of the sphere [2–9]. This uncertainty may be up to a few percent in the measured luminous flux, and consequently in the obtained luminous efficacy, which describes the energy efficiency of the lighting product. With LED lamps superseding typically more uniform incandescent sources, the necessity for the spatial correction has increased when testing new products.

Angular intensity distributions are traditionally measured using goniophotometers [10]. In general, these instruments consist of a detector and rotary elements allowing measurements of luminous intensity of the device under test (DUT) in 4π-solid-angle geometry. Depending on the angular resolution, these types of measurements can be very time consuming, often requiring several hours for each DUT. Furthermore, goniophotometers are usually expensive and require a large amount of dedicated laboratory space: besides the footprint and the floor-to-ceiling height required by the instrument, a non-obscured line of sight must be ensured between the DUT and the detector.

To avoid the laborious goniophotometric measurements, alternative methods have been proposed to take into account spatial non-uniformities of integrating spheres. These methods include the use of a six-port integrating sphere [11, 12], a directional luminous flux standard lamp [13], or fisheye-lens cameras [14, 15].

In this paper, the fisheye camera method [15] for determining spatial non-uniformity corrections is validated by measuring the relative angular intensity distributions of six LED lamps in eight integrating spheres using the camera method, and comparing the correction factors with those obtained using five goniophotometers of different types. In addition to studying the spatial correction factors for luminous flux measurements, the angular intensity distributions obtained using the two methods are also directly compared.

2. Methods and materials

2.1. Overview of the fisheye camera method

The fisheye camera method [15] consists of four main steps: image acquisition, image processing, sphere reconstruction, and determining the relative angular intensity distribution from the reconstruction. First, an image is captured through a port of the integrating sphere, which is illuminated by the DUT installed at the centre of the sphere. Then, the image is divided by a reference image to reduce the impact of camera and sphere imperfections. For the reference image, the sphere is illuminated as evenly as possible. Using the processed image and the intrinsic parameters of the camera, the three-dimensional coordinates are calculated for the image pixels to map them back to the sphere surface. Finally, by subtracting the diffuse light level from this mathematically reconstructed sphere, the relative angular intensity distribution emitted by the source inside the sphere is obtained.

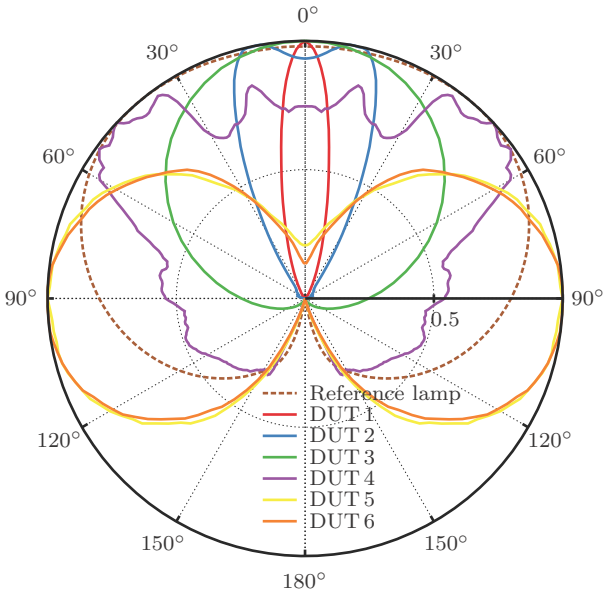

Figure 1. Relative angular intensity distributions of the six DUTs used in the study, and the reference lamp employed for the fisheye camera method. The figure shows the median values of each angular distribution about their optical axis, measured with a mirror goniophotometer.

Ideally, for the reference image, the sphere would be illuminated by an isotropic source. In this study, an LED lamp was employed as the reference. To reduce the impact of the non-uniformity of the reference lamp, a correction was applied to the pixel intensity values of the reprojected image $G(\theta, \phi)$ before subtracting the diffuse light level. The θ and ϕ are the zenith and azimuth angles of the spherical coordinate system, respectively. In this correction, the sum of the relative angular intensity distribution of the reference lamp $I_{\mathrm{ref}}(\theta, \phi)$ and the approximated diffuse light level inside the sphere $\tilde{D}_{\mathrm{ref}}$ is used to multiply the pixel intensity values $G(\theta, \phi)$ according to

$$\begin{aligned} G'(\theta,\phi) &= (I_{\mathrm{ref}}(\theta,\phi) + \tilde{D}_{\mathrm{ref}}) \cdot G(\theta,\phi) \\ &= (I_{\mathrm{ref}}(\theta,\phi) + \tilde{D}_{\mathrm{ref}}) \cdot \frac{I_{\mathrm{DUT}}(\theta,\phi) + D_{\mathrm{DUT}}(\theta,\phi)}{I_{\mathrm{ref}}(\theta,\phi) + D_{\mathrm{ref}}(\theta,\phi)}. \end{aligned} \quad (1)$$

The $D_{\mathrm{DUT}}(\theta, \phi)$ and $D_{\mathrm{ref}}(\theta, \phi)$ are the diffuse light levels inside the sphere, illuminated by the DUT and the reference lamp, respectively. $\tilde{D}_{\mathrm{ref}}$ needs to be determined once for the sphere and the employed reference lamp by, for example, measuring another lamp with a known, broad angular intensity distribution, and adjusting the value of $\tilde{D}_{\mathrm{ref}}$. For an isotropic reference source, the denominator of equation (1) would be a constant scalar, and thus the correction is not required.

2.2. Test lamps

Figure 1 shows the relative angular intensity distributions of the six LED lamps selected for the study as DUTs, as well as

Table 1. Mean closeness scores C of equation (2) calculated for the relative angular intensity distributions measured using each goniophotometer and compared to the other four.

	Goniophotometer					
DUT	1	2	3	4	5	Mean
1	96.2	96.1	96.8	96.7	93.8	95.9
2	94.8	94.4	94.3	96.2	96.2	95.2
3	98.8	99.1	99.0	99.1	98.4	98.9
4	96.5	97.2	97.1	96.9	97.1	97.0
5	95.0	95.9	96.8	96.3	96.8	96.2
6	95.0	95.8	96.9	96.5	96.8	96.2
Mean	96.0	96.4	96.8	97.0	96.5	96.6

that of the reference LED lamp used for the fisheye camera method in this study.

The distributions of the DUTs varied from a very concentrated LED spot (DUT 1) to two broadly radiating, filament-type LED lamps with clear glass bulbs (DUTs 5 and 6). One filament of DUT 6 was significantly dimmer than the other three filaments, resulting in an asymmetrical angular distribution about the optical axis. Additionally, DUT 6 displayed conspicuous flicker. DUT 2 was a spot-type lamp with a mechanically crooked E27 base, which traditionally would cause an unpredictable optical axis orientation inside the sphere. DUT 3 was close to a Lambertian emitter. DUT 4 had a crown-shaped light dispersion element, resulting in a fine-structured angular distribution.

In the initial study [15], the group of test lamps included only DUTs that were rotationally uniform about their optical axis. Thus, it was possible to use the median values to represent each step of deviation from the beam centre. In this study, employing the median values for accurate comparison of the distributions was not applicable for DUTs 2 and 4–6.

2.3. Comparison of angular intensity distributions

For goniophotometric measurements, two direct, two mirror, and one robot [16] goniophotometer were employed. The minimum angular resolution was defined for measuring each DUT, but the participating laboratories were free to increase the resolution at will. The DUTs were allowed to stabilise according to IES LM-79-8 [17] before the goniophotometric measurements. For the fisheye camera method, this stabilisation period was not necessary, because of the simultaneous nature of the data capture. All the angular intensity distribution data were interpolated to the same resolution for calculating the spatial non-uniformity correction factors and the direct comparison of the distributions.

The differences between the relative angular intensity distributions were quantified by a closeness score similar to that in [18], and calculated as

$$C = 100 \cdot \left(1 - \sqrt{\frac{\int_\phi \int_\theta \left(I_i(\theta,\phi) - I_j(\theta,\phi)\right)^2 \sin(\theta)\,\mathrm{d}\theta\,\mathrm{d}\phi}{\int_\phi \int_\theta \left(I_i(\theta,\phi) + I_j(\theta,\phi)\right)^2 \sin(\theta)\,\mathrm{d}\theta\,\mathrm{d}\phi}}\right), \quad (2)$$

where $I_i(\theta,\phi)$ and $I_j(\theta,\phi)$ are the two relative angular intensity distributions being compared with each other. Angle $\theta = 0°$ is parallel with the optical axis of the DUT. Unlike the closeness score calculation in [18], the spherical data were weighted by $\sin(\theta)$ to account for the higher density of the data points close to the optical axis of the DUT [19]. The distributions were rotated about the optical axis ($\phi = 0 \ldots 360°$), and scaled for the best match. The closeness score of 100 would correspond to a perfect match, and 0 to a complete mismatch, i.e. the two light sources emit in completely different directions.

Table 1 shows the mean closeness scores calculated for the relative angular intensity distributions obtained using the five goniophotometers. Each measured distribution of every DUT was compared with the results of the other four goniophotometers for the same DUT, and the mean score was calculated.

Table 2. Integrating spheres employed in the measurements.

Sphere	Diameter (m)	ρ (%)	Baffled camera
1	3.00	95	No (+Yes)
2	4.00	89	Yes
3	2.00	80	Yes
4	1.65	98	Yes
5	1.90	97	No
6	3.00	90	No
7	1.50	87	Yes
8	2.50	95	No

2.4. Integrating spheres

The key parameters of the eight spheres used in the measurements are presented in table 2. The diameters of the spheres ranged from 1.5 m to 4.0 m, and the nominal reflectance factors ρ of the sphere coatings from 80% to 98%. In the initial study [15], the camera port was shaded by a baffle. In these validation measurements, integrating spheres equipped with baffled and non-baffled camera ports were employed. In sphere 1, the measurements of the DUTs were performed in both baffle configurations. When capturing the images without a camera port baffle, the region with the DUT was excluded when searching for the maximum viable exposure time. This area, overexposed by the lamp, was then interpolated using the neighbouring areas.

Figure 2 shows the spatial responsivity distribution functions (SRDFs) of the employed integrating spheres, measured using a sphere scanner [20]. The zenith angles $\theta = 0°$ and $\theta = 180°$ correspond to the top and the bottom of each sphere, respectively. In all the SRDFs, the azimuth angle $\phi = 0°$ points directly to the opposite wall from the camera port.

Figure 3 shows the fisheye camera photographs of the eight integrating spheres. In all the images the sphere is illuminated by the almost Lambertian DUT 3. In sphere 3, which is the sphere with the lowest reflectance factor ρ, the relative angular intensity distribution of the DUT can be roughly distinguished from the raw photograph.

In sphere 2, the DUTs were measured in the base down orientation mounted on a large lamp holder (dark area in the vicinity of $\theta = 180°$ in figure 2). In that sphere, the top-mounted holder of the camera port baffle shaded a small portion of the area of the first reflection. In all the other spheres,

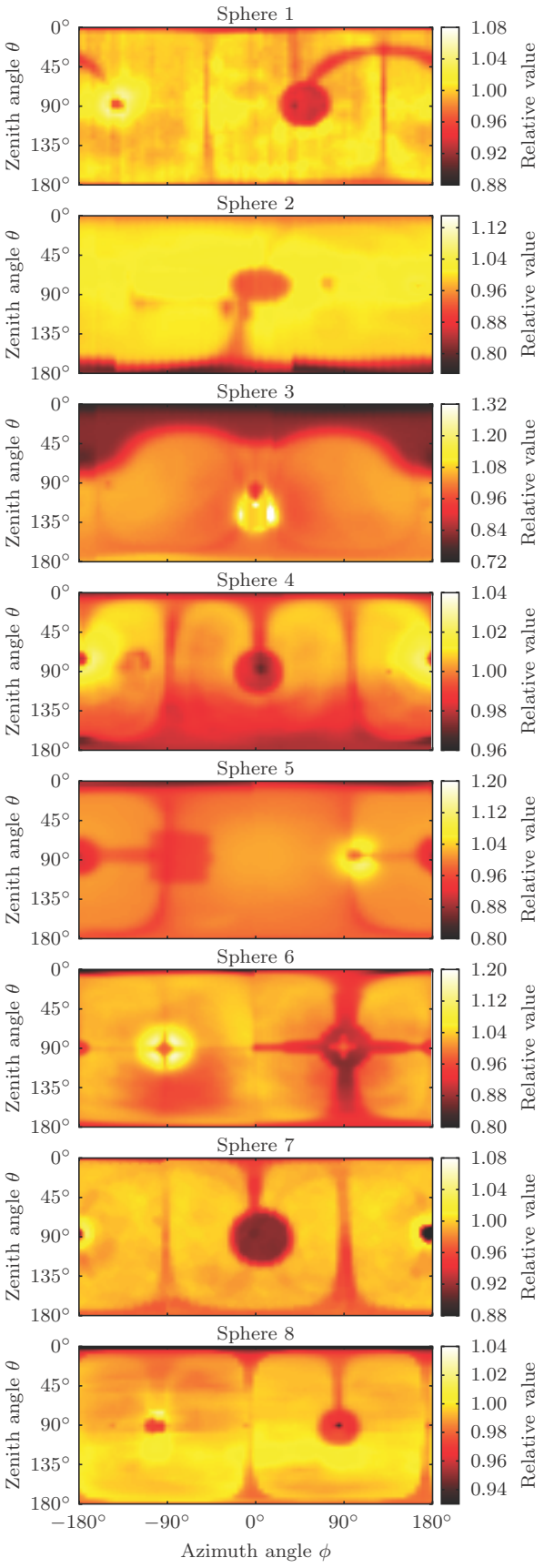

Figure 2. Spatial responsivity distribution functions $K(\theta, \phi)$ of the eight integrating spheres employed in the study.

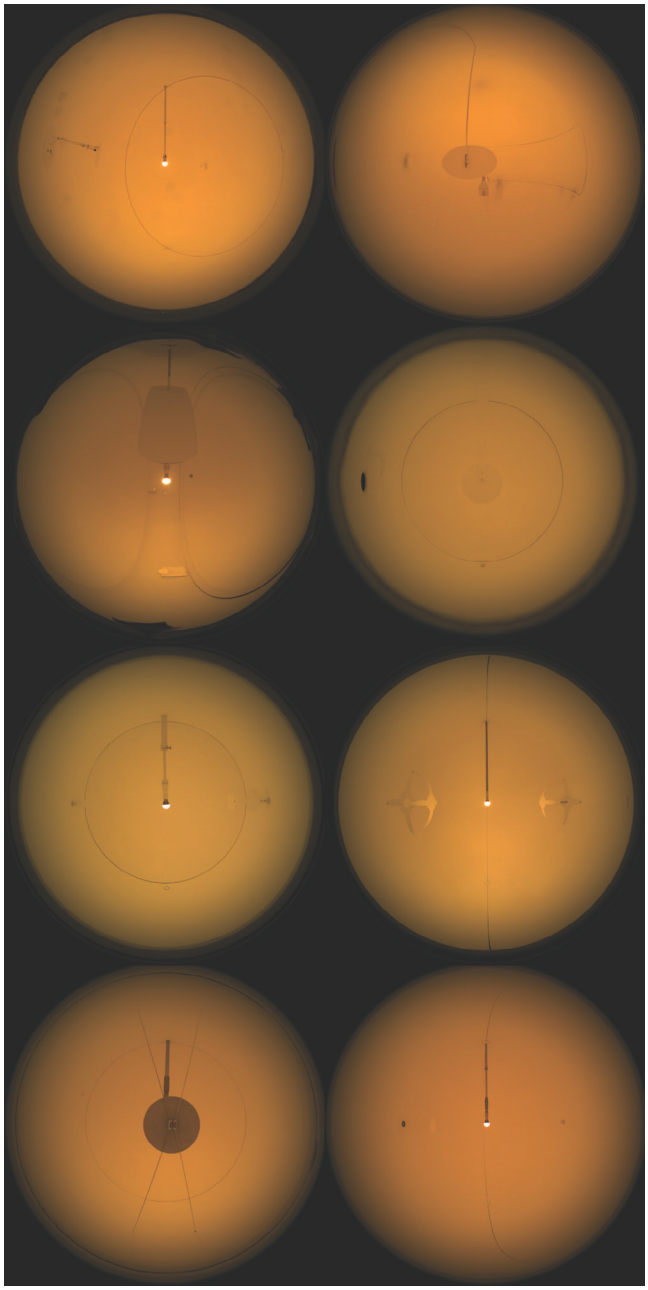

Figure 3. Fisheye camera photographs of the integrating spheres used in the study. On the left from top to bottom spheres 1, 3, 5, and 7, respectively, and on the right from top to bottom spheres 2, 4, 6, and 8, respectively. In all the images, the sphere is illuminated by DUT 3.

the DUTs were measured base up. Sphere 3 had a large baffle in front of the camera, obscuring the lamp holder and a large part of the top hemisphere but not the DUT itself. In spheres 1 and 3, the camera ports were 10° and 15° below the equatorial plane of the spheres, respectively.

For integrating spheres which are calibrated using a luminous flux standard lamp installed inside the sphere, the spatial non-uniformity correction factors are calculated using the equation

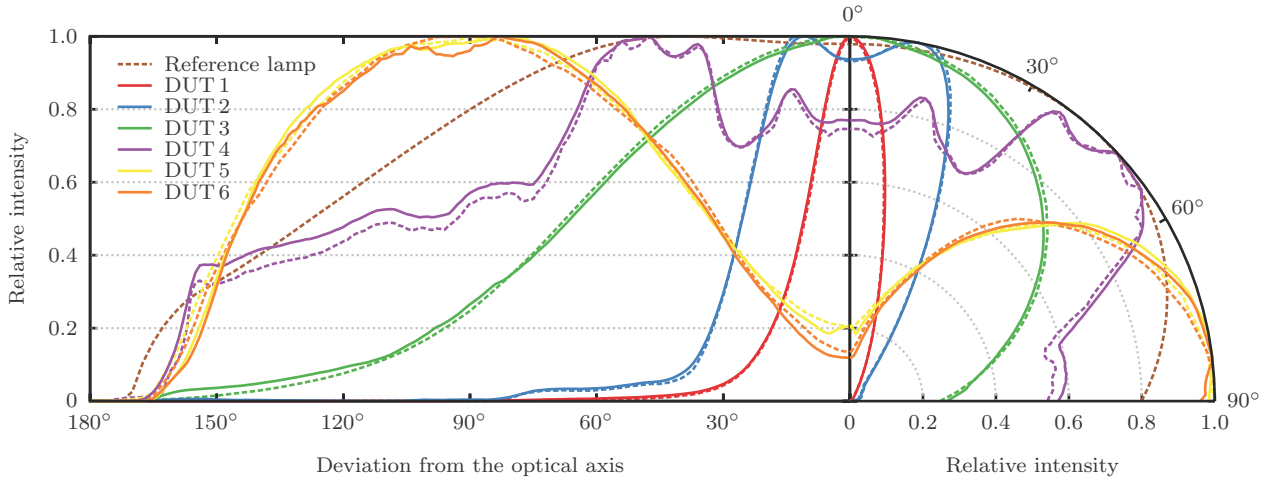

Figure 4. Comparison of the relative angular intensity distributions obtained using the fisheye camera method (solid lines) and a mirror goniophotometer (dashed lines). The camera data are from sphere 1. The goniophotometric data are the same as in figure 1.

Table 3. Mean closeness scores for the relative angular intensity distributions obtained using the fisheye camera method when compared with the five goniophotometers.

DUT	Sphere 1	Sphere 2	Sphere 3	Sphere 4	Sphere 5	Sphere 6	Sphere 7	Sphere 8	Mean
1	96.2	95.4	95.8	95.8	95.9	96.2	95.6	96.2	95.9
2	94.9	93.7	94.4	93.4	94.9	93.9	93.2	94.0	94.0
3	98.1	97.0	97.1	97.8	97.9	97.4	95.8	98.4	97.4
4	96.7	95.8	80.5	91.9	95.9	96.3	95.2	96.0	93.5
5	96.2	93.5	91.7	92.9	95.1	94.1	95.8	93.6	94.1
6	95.1	93.5	93.0	87.5	93.8	92.9	92.8	92.8	92.7
Mean	96.2	94.8	92.1	93.2	95.6	95.1	94.7	95.2	94.6

$$k_{\mathrm{s}} = \frac{\int_{\phi}\int_{\theta} K(\theta,\phi)\, I_{\mathrm{std}}(\theta,\phi)\, \sin(\theta)\, \mathrm{d}\theta\, \mathrm{d}\phi}{\int_{\phi}\int_{\theta} K(\theta,\phi)\, I_{\mathrm{DUT}}(\theta,\phi)\, \sin(\theta)\, \mathrm{d}\theta\, \mathrm{d}\phi} \cdot \frac{\int_{\phi}\int_{\theta} I_{\mathrm{DUT}}(\theta,\phi)\, \sin(\theta)\, \mathrm{d}\theta\, \mathrm{d}\phi}{\int_{\phi}\int_{\theta} I_{\mathrm{std}}(\theta,\phi)\, \sin(\theta)\, \mathrm{d}\theta\, \mathrm{d}\phi}, \quad (3)$$

where $K(\theta,\phi)$ is the SRDF of the sphere, and $I_{\mathrm{DUT}}(\theta,\phi)$ and $I_{\mathrm{std}}(\theta,\phi)$ are the relative angular intensity distributions of the DUT and the luminous flux standard lamp, respectively. For those spheres where the standard lamp and DUTs are operated using different sphere configurations, the SRDF should be scanned for the standard lamp and the DUT configuration separately.

For the comparison of the fisheye camera method and the goniophotometrically obtained spatial correction factors, the SRDF of integrating sphere 4 was used for all the angular distributions. A single sphere map was employed to allow the direct comparison of the correction factors calculated for the angular intensity distributions obtained in different spheres. All the correction factors in this comparison were calculated using equation (3) with an assumption of isotropic $I_{\mathrm{std}}(\theta,\phi)$, despite the fact that the luminous flux standard lamps used to calibrate the spheres have various angular distributions. For every DUT, the angular intensity distributions were also rotated into the same orientation about the optical axis.

In order to find out the magnitude range of the spatial corrections for the employed spheres and DUTs, and thus to get an estimate for the uncertainty associated with the spatial non-uniformity of the spheres, all the correction factors were also calculated using all the eight SRDFs. All the angular data were aligned with the vertical axis of the spherical coordinate system ($\theta = 0°$ for sphere 2, and $\theta = 180°$ for the other spheres), even though in some of the spheres, and especially for DUT 2, the optical axes of the DUTs deviated significantly from the bottom of the sphere: up to 13.6° for DUT 2 in sphere 4. Unlike with the goniometrically obtained angular data, using the fisheye camera method this misalignment could be taken into account with no extra measurements when calculating the spatial non-uniformity correction factor, since the orientation of the optical axis can be determined from the image.

3. Results

3.1. Relative angular intensity distributions

Figure 4 shows the comparison of the relative angular intensity distributions of the six DUTs obtained using the fisheye camera method in sphere 1 and mirror goniophotometer 4. The data used for the visualisation are the median values about the optical axis of the DUTs. For DUT 4, the diffuse light level inside the sphere was underestimated, which resulted in a positive offset in the determined angular distribution.

Table 3 shows the mean closeness scores, calculated using equation (2), for the angular intensity distributions obtained

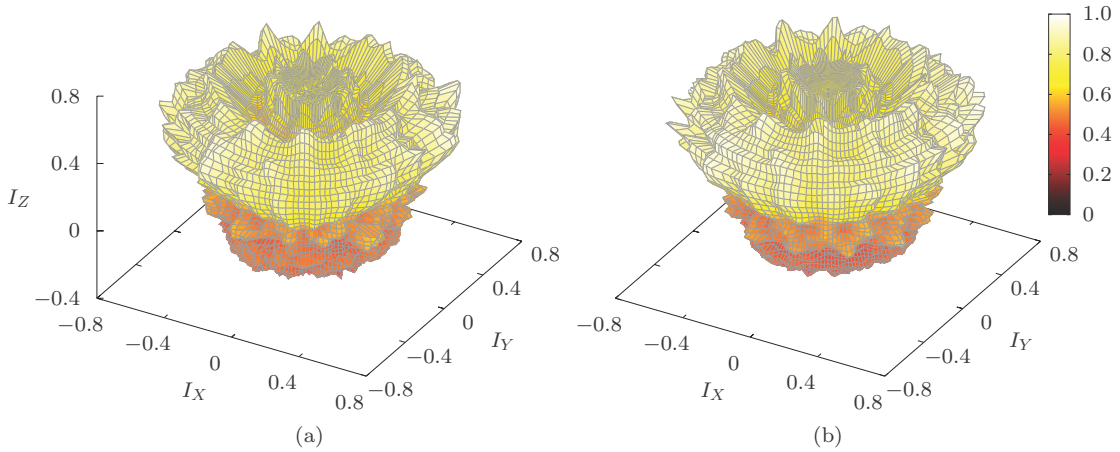

Figure 5. Comparison of the relative angular intensity distributions of DUT 4 obtained using (a) the fisheye camera method in sphere 1 and (b) a mirror goniophotometer. I_X, I_Y, and I_Z are the angular intensity distribution components in X, Y, and Z directions, respectively. Axis Z is parallel to the optical axis of the DUT. The closeness score is 97.6 for these two distributions.

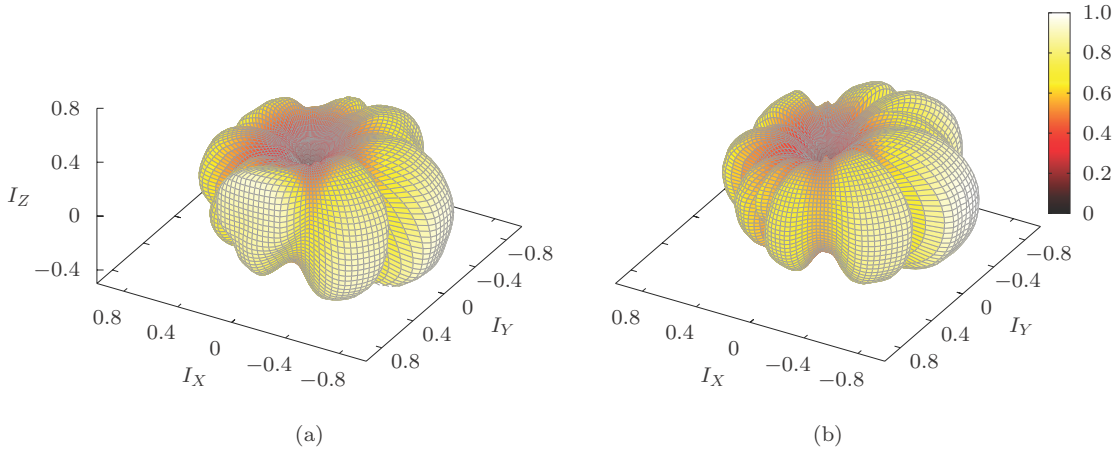

Figure 6. Comparison of the relative angular intensity distributions of DUT 6 obtained using (a) the fisheye camera method in sphere 4 and (b) a mirror goniophotometer. The camera port baffle, round shape in (a) at $(I_X, I_Y) = (0, 0.6)$, and its holder have had a negative impact on the determined distribution. The closeness score is 87.3 for these two distributions.

using the fisheye camera method in all the eight spheres, when compared with the five goniophotometers. The average closeness score for all the DUTs and spheres was 94.6. For comparison, the mean for all the cross-calculated closeness scores for the goniophotometrically obtained angular distribution data was 96.6 (table 1).

The lowest average score resulted from sphere 3. This was caused by the large baffle in front of the camera port. In order to be able to estimate the diffuse light level inside the sphere, the camera needs a view of at least some part of the sphere not illuminated directly by the DUT. For lamps with wide intensity distribution, such as DUTs 4–6, such an area can only be found in the direction of the base of the lamp (see figure 1). In sphere 3, this area is not visible to the camera, due to the large baffle covering the top of the sphere. In sphere 3, the closeness scores for DUTs 5 and 6 are considerably higher than for DUT 4, because these two lamps had low emission also into the direction of their optical axis (figure 1), and thus the error in the diffuse light level estimation was smaller than for DUT 4.

Figures 5 and 6 present the measured relative angular intensity distributions of DUTs 4 and 6, respectively. These types of distributions are particularly challenging for the fisheye camera method, because the non-uniformity of the reference lamp and the residues of the image processing have a larger impact on omnidirectional lamps than on directional ones. Also, the impact of the camera port baffle cannot be eliminated by assuming the rotational uniformity about the optical axis. The distribution in figure 5 obtained using the fisheye camera method was measured in integrating sphere 1, which is a large sphere without a camera port baffle. The camera result in figure 6 was measured in sphere 4, which was equipped with such a baffle. After DUT 4 in sphere 3, this was the sphere-DUT combination with the lowest closeness score. In sphere 4, the fisheye camera method suffers from the camera port baffle, whose round shape can be seen in the foreground of figure 6(a), and the baffle holder, which interferes with determining the diffuse light level in the image by concealing the very top of the sphere.

In general, when measuring broad-distribution DUTs for which rotational uniformity about their optical axis cannot be employed, a baffle in front of the camera will result in two baffle-shaped artefacts in the obtained distribution; one at

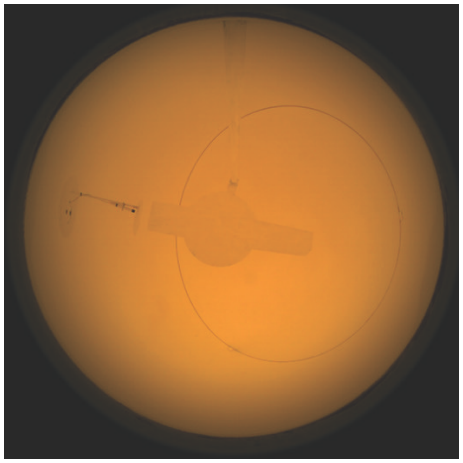

Figure 7. Sphere 1 with a baffle installed in front of the camera.

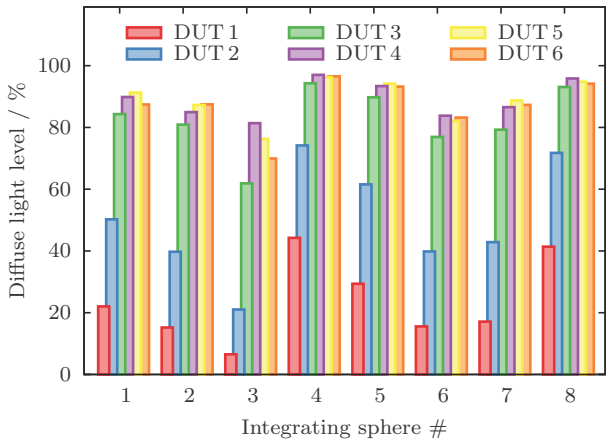

Figure 8. Diffuse light levels in the eight spheres when measuring the six DUTs.

$\phi = 0°$ and another at $\phi = 180°$. This was the case for DUTs 4–6 in spheres 2–4 and 7. Concurrently, for such omnidirectional distributions as those of DUTs 4–6, the impact of errors in the determined angular intensity distributions on the spatial correction factors is usually smaller than for directional lamps.

Figure 7 shows sphere 1 with a baffle installed in front of the camera port. The camera port baffle decreased the mean closeness score of that sphere from 96.2 to 95.4. The scores for directional DUTs were decreased by less than 0.3 on average, but the closeness scores for DUTs 5 and 6 decreased from 96.2 to 94.7 and from 95.1 to 92.3, respectively.

In the case of all the spheres and DUTs, omitting the reference lamp non-uniformity correction of equation (1) would decrease the average closeness score from 94.6 to 87.5. Without the correction, employing a more uniform, frosted incandescent lamp as the reference, instead of the LED lamp shown in figure 1, would still yield the average closeness score of 91.9. With the incandescent reference lamp, the decrease in the mean closeness score stemmed mainly from the results for DUT 4.

Figure 8 shows the diffuse light intensity levels when the relative angular intensity distributions of the six DUTs were

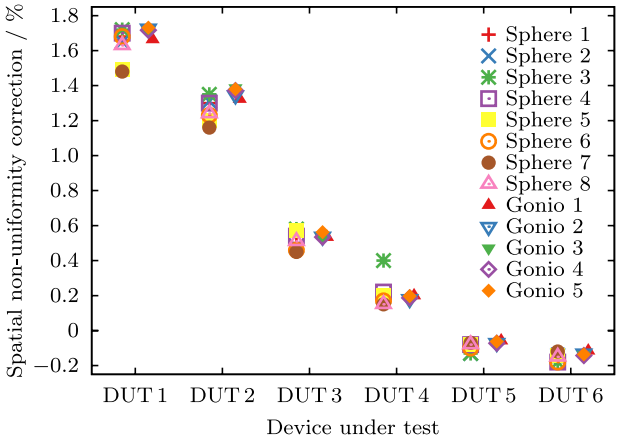

Figure 9. Spatial non-uniformity corrections $(k_s - 1) \cdot 100\%$ calculated for the six DUTs and the SRDF of sphere 4 using the angular intensity distributions measured with the fisheye camera method in all the eight integrating spheres (left-hand points) and with the five goniophotometers (right-hand points).

determined in each sphere. These light levels were subtracted from the corrected image reprojections $G'(\theta, \phi)$ to obtain the distributions. The higher the subtracted diffuse light level, the smaller is the bit depth of the remaining useful signal. It was found that the more concentrated the angular intensity distribution of the DUT, the higher the ratio of the first reflection to the diffuse light level inside the sphere. There was also strong correlation between the mean diffuse light levels and the nominal reflectance factors of the integrating spheres (correlation coefficient 0.92). Aspects such as contamination, and amount and type of structural elements also affect diffuse light levels. The reflectance factor measured for sphere 8 was close to 98%; notably higher than the nominal value of 95%.

If the integrating sphere does not have large structural elements distorting the obtained distributions directly, estimation of the diffuse light level within the sphere, which can also be affected by the sphere elements, is the limiting factor for the accuracy of the fisheye camera method.

3.2. Spatial non-uniformity correction factors

Figure 9 shows the spatial non-uniformity corrections, $(k_s - 1) \cdot 100\%$, calculated using the SRDF of sphere 4 and the relative angular intensity distributions of the six DUTs measured in all the eight spheres. The figure also shows the spatial corrections for the same sphere calculated with the angular distributions obtained using the five goniophotometers. On average, the difference

$$\Delta k_s = \frac{k_{s,\mathrm{camera}} - \bar{k}_{s,\mathrm{gonio}}}{\bar{k}_{s,\mathrm{gonio}}} \cdot 100\% \qquad (4)$$

between the two measurement methods was 0.05%. The $\bar{k}_{s,\mathrm{gonio}}$ in equation (4) indicates the mean spatial correction factor calculated for the DUT with the angular data obtained using the five goniophotometers. The maximum difference in the spatial correction factors obtained using the two methods was 0.22%, which resulted from DUT 1 in sphere 7. Employing a frosted incandescent lamp as the reference lamp,

Table 4. Spatial non-uniformity corrections $(k_s - 1) \cdot 100\%$ obtained for the six DUTs in the eight integrating spheres using the fisheye camera method. The table also shows the differences Δk_s to the mean results of the five goniophotometers (in parenthesis). The value for DUT 4 in sphere 3 is an outlier for the reasons explained in section 3.1. The range of the corrections is expressed as the difference between the maximum and the minimum correction for each sphere.

DUT	Sphere 1	Sphere 2	Sphere 3	Sphere 4	Sphere 5	Sphere 6	Sphere 7	Sphere 8 (%)
1	−0.10	1.50	−0.10	1.71	1.04	1.33	0.32	0.06
	(0.02)	(−0.10)	(0.11)	(0.02)	(−0.15)	(0.03)	(−0.05)	(0.01)
2	−0.32	0.49	0.24	1.29	0.73	0.89	0.06	−0.08
	(−0.02)	(−0.07)	(0.07)	(−0.07)	(0.02)	(−0.10)	(−0.01)	(0.02)
3	−0.15	−0.24	−1.14	0.54	0.09	0.70	0.05	−0.22
	(0.02)	(0.01)	(−0.18)	(0.00)	(0.02)	(−0.06)	(−0.01)	(0.01)
4	−0.01	−0.14	−1.31	0.15	−0.05	0.39	0.04	−0.11
	(0.02)	(0.01)	(−1.16)	(−0.03)	(−0.02)	(0.00)	(0.06)	(0.01)
5	0.07	−0.00	−0.17	−0.08	−0.20	0.03	0.02	0.00
	(0.03)	(0.01)	(−0.00)	(−0.00)	(−0.06)	(−0.03)	(0.02)	(0.01)
6	0.02	−0.03	−0.70	−0.07	−0.15	0.12	0.06	−0.00
	(0.02)	(−0.05)	(−0.23)	(−0.01)	(−0.10)	(−0.04)	(0.10)	(0.03)
Range	0.39	1.74	1.54	1.80	1.24	1.30	0.30	0.27

without the correction of equation (1), would slightly increase the average difference between the methods to 0.06%.

The spatial corrections obtained with the fisheye camera method and the rest of the SRDFs are shown in table 4. The table also shows the differences to the mean spatial correction factors $\bar{k}_{s,\,\mathrm{gonio}}$ calculated with the angular intensity distribution data from the goniophotometers. The spatial correction range for each sphere shows that the necessity for the correction cannot be determined solely from the range of the SRDF values.

4. Conclusion

In this paper, the fisheye camera method was validated by comparing its results in eight integrating spheres to those of five goniophotometers. The closeness scores, describing the similarity between any two relative angular intensity distributions, were calculated to compare the distributions of six LED lamps measured using the two methods. Additionally, the spatial non-uniformity correction factors were calculated for the DUTs using the spatial responsivity map of one sphere, to allow comparison of the methods. The spatial correction factors were also calculated using the respective spatial responsivity maps of all the eight spheres to see the magnitude range of the corrections.

When comparing all the relative angular intensity distributions obtained using the fisheye camera method with those obtained using the goniophotometers, the average closeness score was 94.6 out of 100. The average, cross-calculated closeness score for the angular intensity distributions obtained using the five goniophotometers was 96.6. The highest mean for one sphere and the six DUTs was 96.2. Out of the five goniophotometers, the highest average closeness score was 97.0.

The maximum difference between the two methods in the spatial corrections calculated using the SRDF of one sphere was 0.22%, with the average difference being 0.05%. The mean spatial corrections, obtained using the goniophotometers, for the six DUTs and all the eight integrating spheres ranged from −0.96% (DUT 3 in sphere 3) to 1.69% (DUT 1 in sphere 4).

It was found that the lower the reflectance factor of the sphere coating, the higher is the signal-to-noise ratio for measuring the relative angular intensity distributions. The main cause for the differences in the obtained distributions were those sphere structures which prevented accurate estimation of the diffuse light level inside the sphere. Fortunately, this is mainly a problem for DUTs with omnidirectional angular intensity distributions, which typically require smaller spatial non-uniformity corrections than directional lamps.

Acknowledgment

The work leading to this study is partly funded by the European Metrology Programme for Innovation and Research (EMPIR) Project 15SIB07 PhotoLED 'Future Photometry Based on Solid State Lighting Products'. The EMPIR initiative is co-funded by the European Union's Horizon 2020 research and innovation programme and the EMPIR Participating States. For assisting in the measurements, the authors thank M F Y Ali, J Askola, C Dam-Hansen, K Drbalkova, D D Corell, C P E C Geluk, M Hirschberg, L Kallenbach, N Leise, J Linden, R Maass, M Meyer, M Taddeo, and N Wagner. A Kokka acknowledges the funded position of Aalto ELEC doctoral school and the support of the Tutkijat Maailmalle program.

ORCID iDs

Anders Thorseth https://orcid.org/0000-0003-4344-0770
Tuomas Poikonen https://orcid.org/0000-0001-9970-5550

References

[1] International Commission on Illumination 1989 The measurement of luminous flux *Technical Report CIE* No. 84

[2] Ohno Y 1996 Realization of NIST 1995 luminous flux scale using integrating sphere method *J. IES* **22** 13–22
[3] Ohno Y, Lindemann M and Sauter G 1997 Analysis of integrating sphere errors for lamps having different angular intensity distributions *J. Illum. Eng. Soc.* **26** 107–14
[4] Ohno Y 1998 Detector-based luminous-flux calibration using the absolute integrating-sphere method *Metrologia* **35** 473–8
[5] Lahti K *et al* 2000 Realization of the luminous-flux unit using a LED scanner for the absolute integrating-sphere method *Metrologia* **37** 595–8
[6] Ohno Y and Daubach O 2001 Integrating sphere simulation on spatial non-uniformity errors in luminous flux measurement *J. Illum. Eng. Soc.* **30** 105–15
[7] Hovila J, Toivanen P and Ikonen E 2004 Realization of the unit of luminous flux at the HUT using the absolute integrating-sphere method *Metrologia* **41** 407–13
[8] Poikonen T *et al* 2012 Luminous efficacy measurement of solid-state lamps *Metrologia* **49** S135–40
[9] Kim Y-W, Lee D-H, Park S-N, Jeon M-Y and Park S 2012 Realization and validation of the detector-based absolute integrating sphere method for luminous-flux measurement at KRISS *Metrologia* **49** 273–82
[10] International Commission on Illumination 1996 The photometry and goniophotometry of luminaires *Technical Report CIE* No. 121
[11] Park S, Lee D-H and Park S-N 2011 Six-port integrating sphere photometer with uniform spatial response *Appl. Opt.* **50** 2220–7
[12] Park S, Lee D-H, Park S-N and Park C-W 2013 Experimental validation of the six-port design for a highly uniform integrating sphere photometer *Appl. Opt.* **52** 7178–85
[13] Yu H-L and Liu W-C 2013 Total luminous flux measurement for flexible surface sources with an integrating sphere photometer *Meas. Sci. Technol.* **25** 015012
[14] Zong Y 2015 Development of a new sphere-goniophotometer method *28th CIE Session 2015—Abstracts* pp 147
[15] Kokka A, Pulli T, Poikonen T, Askola J and Ikonen E 2017 Fisheye camera method for spatial non-uniformity corrections in luminous flux measurements with integrating spheres *Metrologia* **54** 577–83
[16] Lindemann M, Maass R and Sauter G 2015 Robot goniophotometry at PTB *Metrologia* **52** 167–94
[17] Illuminating Engineering Society 2014 Electrical and photometric measurements of solid-state lighting products *Technical Report IES* LM-79-8
[18] Bergen T 2012 A practical method of comparing luminous intensity distributions *Lighting Res. Technol.* **44** 27–36
[19] Gassmann F, Krueger U, Bergen T and Schmidt F 2017 Comparison of luminous intensity distributions *Light. Res. Technol.* **49** 62–83
[20] Winter S, Lindemann M, Jordan W, Binder U and Anokhin M 2009 Convenient integrating sphere scanner for accurate luminous flux measurements *Metrologia* **46** S248–51